REPORT DOCUMENTATION PAGE

Form Approved OMB NO. 0704-0188

1. REPORT DATE (DD-MM-YYYY)	2. REPORT TYPE	3. DATES COVERED (From - To)
24-08-2015	Book Chapter	-

4. TITLE AND SUBTITLE
Advanced Optical Fibers for High power Fiber lasers

5a. CONTRACT NUMBER
W911NF-10-1-0423

5b. GRANT NUMBER

5c. PROGRAM ELEMENT NUMBER

6. AUTHORS
Liang Dong

5d. PROJECT NUMBER

5e. TASK NUMBER

5f. WORK UNIT NUMBER

7. PERFORMING ORGANIZATION NAMES AND ADDRESSES
Clemson University Research Foundation
Office of Sponsored Programs
Clemson University Research Foundation
Clemson, SC 29631 -0946

8. PERFORMING ORGANIZATION REPORT NUMBER

9. SPONSORING/MONITORING AGENCY NAME(S) AND ADDRESS (ES)
U.S. Army Research Office
P.O. Box 12211
Research Triangle Park, NC 27709-2211

10. SPONSOR/MONITOR'S ACRONYM(S)
ARO

11. SPONSOR/MONITOR'S REPORT NUMBER(S)
58391-EL-HEL.45

12. DISTRIBUTION AVAILIBILITY STATEMENT
Approved for public release; distribution is unlimited.

13. SUPPLEMENTARY NOTES
The views, opinions and/or findings contained in this report are those of the author(s) and should not contrued as an official Department of the Army position, policy or decision, unless so designated by other documentation.

14. ABSTRACT
A review of recent fiber developement for high power fiber lasers.

15. SUBJECT TERMS
Fiber lasers, specialty fibers, photonic crystal fibers, photonic bandgap fibers

16. SECURITY CLASSIFICATION OF:			17. LIMITATION OF ABSTRACT	15. NUMBER OF PAGES	19a. NAME OF RESPONSIBLE PERSON
a. REPORT	b. ABSTRACT	c. THIS PAGE			Liang Dong
UU	UU	UU	UU		19b. TELEPHONE NUMBER 864-656-5915

Report Title

Advanced Optical Fibers for High power Fiber lasers

ABSTRACT

A review of recent fiber developement for high power fiber lasers.

Chapter 7

Advanced Optical Fibers for High Power Fiber Lasers

Liang Dong

Additional information is available at the end of the chapter

http://dx.doi.org/10.5772/58958

1. Introduction

The nonlinear limits of conventional single-mode fibers were well recognized in the nineties during the earlier efforts to scale the peak powers of pulsed fiber lasers. These earlier efforts focused on lowering the NA and optimizing the refractive index profile of optical fibers to increase the effective mode area [1, 2]. The emergence of photonic crystal fibers in the late nineties gave new impetus to the mode area scaling of single-mode optical fibers. The observation of the "endlessly single-mode" nature of *photonic crystal fibers* (PCF) at small hole sizes in 1996 [3] led to an early realization of the dispersive nature of a photonic crystal cladding [4], which limits the increase of normalized frequency V at short wavelengths. It was quickly realized that the scalability of Maxwell's equation allows for single-mode operation at a very short wavelengths in a small core to be directly translated into single-mode operation in a large core at longer wavelengths [5]. This led to a rapid progress in scaling of core diameters of single-mode PCF, culminating in the 100μm-core diameter demonstrated in 2006 [6].

The design and fabrication techniques developed for photonic crystal fibers also led to a realization of the potential of optical fibers with more open cladding structures than the closed concentric circles found in conventional optical fibers. It then became possible to design and fabricate leaky waveguides where differential mode losses can be used to control the number of propagation modes. As a consequence, *leakage channel fibers* (LCF) were proposed and first demonstrated in 2005 [7]. Two years later, single-mode operation in a record core diameter of ~180μm was demonstrated in a LCF [8].

Many other approaches based on conventional fibers were also pioneered during the last decade. One notable example is the *chirally coupled core* (CCC) fiber [9, 10], which relies on out-coupling of *higher-order modes* (HOM) to side cores adjacent to the main core. Phase-matching is achieved with the help of angular momentum from the helical side cores, which are formed by spinning the preform during fiber drawing. Another notable example is based on the

propagation of a higher-order mode in a specially designed multimode fiber [11, 12]. It is argued that perturbations mostly have anti-symmetry in optical fibers and promote mode coupling mostly between modes of opposite symmetries. The mode spacing between a radially symmetric LP0n mode and its nearest neighbor modes with opposite symmetry is, in fact, larger for higher order modes. These higher-order modes are also more resistant to bend-induced mode compression. A special fiber design facilitates the ease of mode conversion to and from the LP0n mode using a *long period grating* (LPG).

In this chapter, we will give a brief introduction to the key approaches to effective mode area scaling which have shown great promise for future high power fiber lasers. Basic concepts are introduced and the latest developments are also discussed.

2. Photonic crystal fibers

The authors of the paper in 1996 [3] were looking for photonic bandgap guidance in the defect core of the PCF with a core size of ~4.6 μm. The reason for the absence of photonic bandgap guidance in a solid-core PCF with air holes in the cladding only became clear a few years later. To their surprise, they observed very broadband single-mode guidance from 458–1550 nm (extended to 337-1550 nm in [4]). A conventional single-mode step-index optical fiber would become multimode at shorter wavelength. Even more surprising, the diffraction angle of the output beam was smaller at shorter wavelengths, indicating a smaller fiber numerical aperture at short wavelength.

2.1. Fundamental space-filling mode of photonic crystal cladding

In a follow-on paper [4] the initial observation of the "endlessly single-mode" nature of photonic crystal fibers was explained by the dispersive nature of the cladding, which can be viewed as a composite of two materials, i.e. silica and air. The effective refractive index of the composite cladding was identified for the first time as the effective index of the fundamental mode of the composite cladding, referred to as the *fundamental space-filling mode (FSM)*. In the extreme case of conventional optical fibers with an infinite cladding, the effective index of the fundamental space-filling mode becomes the refractive index of the cladding. In PCFs with air holes, the cladding index n_{cl}, i.e. the effective index of the fundamental space-filling mode, is lower than the refractive index of the background glass n_b due to the existence of the air holes, i.e. $n_{cl}<n_b$. The core index n_{co} is the same as the index of the background glass, $n_{co}=n_b$. Fundamental optical guidance in PCFs can, therefore, in principle, be understood in a similar way to that in conventional optical fibers (see Figure 1).

This paper [4] established the principle for understanding the basic guidance properties of PCFs. In conventional optical fibers, the refractive indexes of core and cladding are only weakly dependent on wavelength due to material dispersion. This is also expected of the core refractive index of a PCF. The refractive index of the composite photonic crystal cladding, however, behaves very differently. At the long wavelength extreme, i.e. $\lambda \to \infty$, the wavelength is much larger than the air holes and the fundamental space-filling mode will occupy all areas

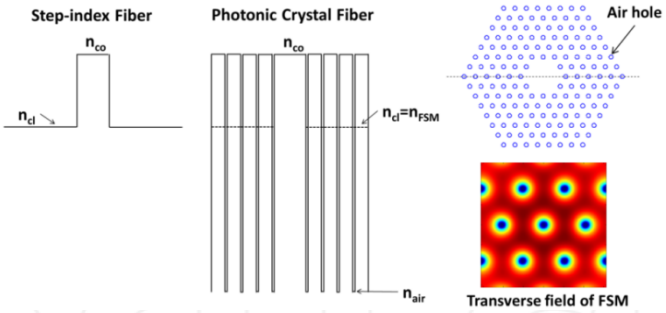

Figure 1. Refractive index of photonic crystal fiber cladding.

of the cladding equally. In this case, the refractive index of the FSM can be obtained by averaging the square of the refractive index of the composite photonic crystal cladding, i.e. $n_{cl}^2=n_b^2(1-F)+n_{air}^2F=n_b^2-F(n_b^2-n_{air}^2)$ where F is the area fraction of air; and n_{air} is the refractive index of air. The effective NA of the PCF for $\lambda\rightarrow\infty$ is, therefore, $F^{1/2}(n_b^2-n_{air}^2)^{1/2}$. At the short wavelength extreme, i.e. $\lambda\rightarrow0$, the wavelength is much smaller than the pitch of the air holes and the fundamental space-filling mode is mostly in the region with high refractive index, i.e. the background glass. In this case, the cladding index is the refractive index of the background glass n_b. The effective NA of a PCF at $\lambda\rightarrow0$ trends to zero. The guidance of a PCF still gets weaker at large λ, as in a conventional optical fiber, due to the inverse wavelength dependence of the normalized frequency V. In addition, its guidance also gets weaker at short wavelengths due to the diminishing NA, which also limits the growth of V and leads to the "endlessly single-mode" nature of the PCFs with small air holes. Guidance of PCF will, therefore, diminish at both long and short wavelength ends, possessing two bend-induced cut-off edges.

2.2. Single mode and multimode regime of photonic crystal fibers

In conventional fibers, a mode is guided when the effective mode index n_{eff} is between the core and cladding index, i.e. $n_{co}>n_{eff}>n_{cl}$. The mode cut-off can be identified when $n_{eff}=n_{cl}$. The second-order mode cuts off in a step-index fiber at V=2.405. In the first reported work on determining the single-mode regime of PCFs with a 1-cell core, i.e. one hole missing at the defect core, by Birks et al [4], a somewhat arbitrary equivalent step-index core radius equaling *pitch*Λ, i.e. center-to-center hole separation, was used to calculate the V value. Work by Saitoh [13] using a *finite element model* (FEM) to determine n_{FSM} and the condition $n_{eff}=n_{cl}$ to determine the second-order mode cut-off, put the effective step-index core radius to be $\Lambda/3^{1/2}$ for a one-cell core. Later work by Saitoh [14] determined the effective step-index core radius to be Λ for a 3-cell core and $2^{1/2}\Lambda$ for a 7-cell core.

The optical waveguide equation allows the scaling of all parameters measured in the length scale by the same factor. For PCF, the most convenient scaling factor is $1/\Lambda$. The second-order mode cut-off is typically plotted as a normalized wavelength λ/Λ versus normalized hole diameter d/Λ plot. This is shown for PCFs with 1-cell, 3-cell and 7-cell core in Figure 2 [14]. For each of the curves, the area above the curve is in the single-mode regime, i.e. the wave-

lengths above the second-order mode cut-off wavelength, and, below it, multimode regime. The "endlessly single-mode" nature of PCFs can be easily identified in Figure 2. When d/Λ<0.424, 0.165 and 0.046 respectively for 1-cell, 3-cell and 7-cell core PCFs, the PCFs will remain in the single-mode regime for all wavelengths. It is worth noting that Figure 2 is for PCFs with infinite cladding. For PCFs with finite cladding, guidance is weaker and the second-order-mode cut-off is expected to happen at slightly shorter wavelengths. The curves in Figure 2 are expected to move downwards slightly. It needs to be noted as discussed earlier, that the PCFs are too weak to guide any light at long and short extremes of wavelength. The critical bend radius at the short wavelength edge is determined to be dependent on pitch Λ and wavelength λ such that [4]

$$R_c \propto \frac{\Lambda^3}{\lambda^2} \tag{1}$$

The critical bend radius at the short length edge increases in proportion to $1/\lambda^2$ as wavelength decreases. This relation was verified experimentally for the critical bend radius at 3dB excessive bend loss [4]. It comes directly from the dispersive nature of the photonic crystal cladding.

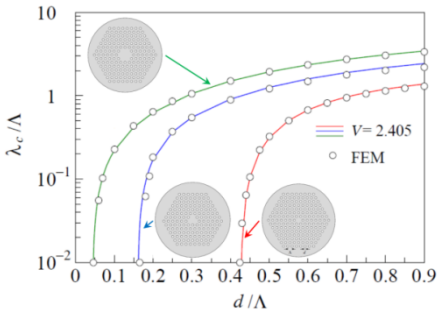

Figure 2. The second-order mode cut-off determined by $n_{eff}=n_{FSM}$ (dots) and V=2.405 (solid lines) using core radius $\varrho=\Lambda/3^{1/2}$, Λ and $2^{1/2}\Lambda$ respectively for 1-cell, 3-cell and 7-cell cores [14].

2.3. Waveguide loss of photonic crystal fibers

PCFs are intrinsically leaky, i.e. there is always a finite waveguide loss for each mode in a PCF with a finite cladding. The waveguide loss can be found by calculating the imaginary part of the effective mode index using a numerical mode solver. When plotting the waveguide loss versus wavelength, the slope is expected to change around cut-off. This can also be used to determine the second-order-mode cut-off. This was done for a 1-cell core PCF [15]. The results are consistent with those in [13].

In conventional optical fibers, the fully enclosed core and cladding boundary ensures that waveguide loss is zero for all guided modes, i.e. those that satisfy the conditions for total

http://dx.doi.org/10.5772/58958

internal reflection at the boundary. For the open structure of PCFs with a finite cladding, all modes are leaky with finite waveguide losses. At the extreme of an infinite number of layers, the waveguide losses are zero. The waveguide losses are lower for larger air holes and can be substantially lowered by increasing the number of air-hole layers. In practice, the waveguide loss can be made below other material and process related losses. By employing appropriate polishing, etching and dehydration processes, a PCF with a loss 0.28dB/km at 1550nm has been demonstrated [16]. For applications in fiber lasers where a length of not more than a few tens of meters is used, the waveguide loss does not present any problem if appropriate designs are used.

2.4. Modeling of photonic crystal fibers

Due to the complexity of the geometrical structures of PCFs, numerical models are typically used to find mode properties including the effective mode index, waveguide loss and effective mode area. For any numerical mode solvers, electric and magnetic fields are described by an expansion series. Eigenvalue equations are then established by requiring the fields to satisfy all boundary conditions. These equations are typically expressed as a set of linear equations, which can be solved for complex effective mode index. The more complex a waveguide design is, the larger is the number of linear equations. The waveguide dispersion can be calculated from the real part of the complex effective mode index. The waveguide loss can be obtained from the imaginary part of the complex effective mode index. Electric and magnetic fields can be calculated once the effective mode index is determined. The most common and flexible numerical mode solver is a *finite element mode solver* (FEM). This is commercially available from COMSOL (*http://www.comsol.com/*). A FEM is capable of handling practically any design. It can, however, be computationally very demanding. If only circular boundaries are involved, a Multipole mode solver is a good option [17, 18]. It is based on the decomposition of fields into circular Bessel series, which are the most accurate and efficient method for modeling circular boundaries. For non-commercial research and teaching purposes, it can be downloaded from the University of Sydney website (*http://sydney.edu.au/science/physics/cudos/research/mofsoftware.shtml*). A plane wave expansion method can also be used. This, however, assumes an infinite cladding and, therefore, cannot determine the waveguide loss.

2.5. Mode area scaling with photonic crystal fibers

The first demonstration of a large-core PCF was performed by Knight el at [5]. The 1-cell PCF with relative hole diameter $d/\Lambda \approx 0.12$ and a core diameter of $2\varrho = 22.5\mu m$, provided robust single-mode guidance at 458nm. According to Figure 2, a 1-cell PCF with $d/\Lambda < 0.424$ is expected to be single-mode over its entire wavelength range. It is, therefore not surprising that the PCF was single mode at 458nm. The critical bend radius was measured to be 50cm at 458nm and 4cm at 1.55μm [5]. This fiber is expected to have a critical bend radius of ~10cm at 1μm using equation 1.

Considering the wavelength scalability of the waveguide equation, this 1-cell PCF with $2\varrho/\lambda \approx 50$ can be scaled by a factor of ~2.2 to a ~50μm core diameter to operate at 1μm. The critical bend radius for this single-mode PCF with 50μm core diameter is expected to be ~1.1m at 1μm

according to equation 1! A similarly scaled 1-cell PCF with a core diameter of 30μm will have a critical bending radius of ~24cm. This is probably close to the practical limit of coiled single-mode 1-cell PCFs. Above a core diameter of ~40μm, 1-cell single-mode PCF can only be used in a straight configuration in practice. The single-mode operation of PCFs with large core diameters comes at the cost of weak guidance as a result of the diminishing effective NA. This fundamentally limits the use of single-mode PCFs with large cores in coiled configurations. If PCFs are allowed to operate in the few-moded regime, coiled PCFs with slightly larger core diameters are possible. For high average power fiber lasers with outputs exceeding kW, effective thermal management becomes increasingly critical. Long fiber lengths of many meters are required. The constraint of not being able to coil the fibers can become a major issue considering the additional space constraints.

2.6. Rare-earth-doped glass for large-core photonic crystal fibers

The diminishing NA of PCFs with large cores also has additional implications, as realized by the authors of [5]. To fabricate rare-earth-doped large-core PCFs, the core refractive index needs to be accurately controlled at levels far below the very small effective index difference between the core and cladding in order not to disturb the guidance properties of the PCFs. This requires much improved techniques for the fabrication of the active core in large-core PCFs.

The first ytterbium-doped large-core PCF with 15μm core diameter was reported in 2001 at Bath University [19]. The effective mode area at 1μm was ~100μm^2. The laser operated in single mode with poor efficiency. The key advance was the use of a repeated stack-and-draw process to achieve a uniformly doped core with a refractive index close to silica. Conventional fabrication techniques for rare-earth doped silica fibers result in significant non-uniformity in refractive index across the core as well as a raised refractive index above silica. Due to the weak guidance in large-core PCFs, any index non-uniformity across the core can lead to mode distortion. It also requires the refractive index of the core to be very close to the silica background in PCFs. The authors of [19] fabricated ytterbium-doped glass with low doping levels. The doped glass is surrounded by some undoped silica glass. The glass is stacked and drawn twice before being finally incorporated into the core of a PCF. The resulting PCF has an ytterbium-doped core which consists of 425 original doped glass sections. The dimension of each of the original doped glass sections is much smaller than the wavelength of light and the core of the PCF, therefore, appears to be homogeneous to light at the operating optical wavelength. The doped core is also heavily diluted by the addition of silica glass (90%), leading to an average refractive index close to that of silica [20]. In the same paper, it was pointed out that rare-earth-doped glass with a higher index can be stacked and drawn with undoped glass with a low index to achieve a better match to that of silica background [20].

2.7. Double-clad photonic crystal fibers with high NA air-clad for pump guidance

The concept of a composite air-glass clad with a high air-filling fraction to provide a high NA pump guide in a double-clad fiber was first proposed in 1999 at what was then then Lucent Technologies [21]. The high pump NA can enable a significant improvement in pump coupling

http://dx.doi.org/10.5772/58958

especially from low brightness multimode diode lasers for a given pump waveguide dimension. In conventional double-clad fibers, low-index polymer coatings are typically used to form the pump cladding. The air-clad pump isolates high pump powers from the polymer coatings, leading to potentially improved reliability.

The first such fiber was demonstrated in 2000, where the pump cladding was mostly air except for a single connecting element [22]. The measured pump NA over 1m was below 0.2. The fiber was passive and there was no laser demonstration in this first attempt. The first cladding-pumping demonstration in an active fiber with an air-clad pump guide and a conventional core design was in 2001 at Southampton University [23]. The measured NA of the pump guide with air-cladding was 0.4-0.5. In a separate demonstration from Southampton University later in the same year, a conventional core with a very low NA together with a photonic crystal cladding was used in combination with a pump guide with air-cladding [24]. The core guidance came from a combination of the raised core index and the photonic crystal cladding. Cladding pumping with a low brightness laser diode at 915nm (100μm core with a NA=0.22) was demonstrated with a slope efficiency of 70% relative to the absorbed pump power. The measured pump NA over a short length (~10cm) was 0.3-0.4. NA over much longer fiber length as in a fiber laser is expected to be lower. The first true active double-clad photonic crystal fibers with a pump air-cladding was demonstrated in 2003 with a measured pump NA of 0.8 at 1μm [20].

The theoretical basis for the high NA of optical waveguides formed by air-cladding was established in [25]. It had been understood previously that the effective index of a glass and air composite can be obtained by the effective index of the fundamental space filling mode. An example of high NA air-clad used in double-clad fibers is shown in Figure 3 from [25]. In such air-glass composites, the glass webs can be considered as slab waveguides. The separations between the webs are typically far enough that the webs can be considered as isolated. In this case, the effective index of the glass-air composite cladding can be well approximated by that of the fundamental slab waveguide mode. This can be easily calculated. The resulting pump NA is only dependent on the ratio of the web width w and wavelengthλ. This is plotted in Figure 3(c), showing that a small w/λ is critical for high NA.

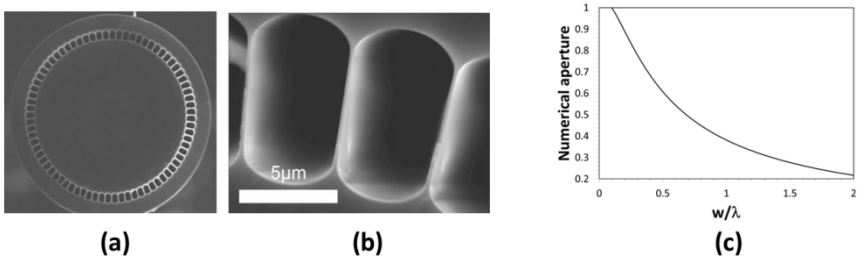

Figure 3. (a) High NA air-clad from [25], (b) close-up of the high NA air-clad, and (c) NA of air-clad waveguide based on slab waveguide model plotted against the ratio of waveguide width w and wavelength λ.

2.8. Progress of active large-core photonic crystal fibers

Since 2003, the group at Friedrich-Schiller-University Jena has been playing a significant role in the development large-mode-area photonic crystal fibers with pump air-clad. In their first work in collaboration with then Crystal Fibre A/S, now NKT Photonics, an ytterbium-doped PCF with effective mode area of ~350μm^2 and mode field diameter (MFD) of 21μm was demonstrated [26] (see Figure 4). The 3-cell PCF had a hole diameter d=2μm and pitch Λ=11.5, giving an d/Λ=0.18. The core diameter was 28μm. A relatively small circular area of 9μm was doped in the 3-cell core. The doped area had a high ytterbium-doping level of ~0.6 at%. It was further co-doped with aluminum and fluorine to provide an index merely 2×10^{-4} above the silica background. The PCF with the raised index in the doped area was simulated, showing that the fiber guides the second-order mode, which is, however, close to cut-off. The fiber had a 150μm pump guide with an air clad. The webs in the air clad were ~50μm long with a thickness of ~390nm, giving w/λ=~0.4 at 976nm. The measured pump NA was 0.55, slightly below the NA=0.68 predicated by the slab model in Figure 3. The fiber had an outer glass diameter of 450μm and was coated with standard acrylic coating. Due to the high doping level, the fiber has a pump absorption of ~9.6dB/m at 976nm. An impressive slope efficiency of 78% was demonstrated with respect to the launched pump power.

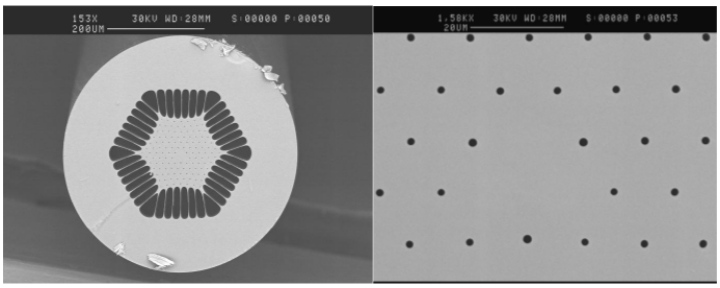

Figure 4. SEM image of the air-clad ytterbium-doped large-mode-area photonic crystal fiber in [26].

In a subsequent paper in 2003 [27], the fiber in [26] and a new fiber with narrower pump air-clad were studied with the FEM for temperature distributions in the fiber at various thermal loads in the core, considering both convective and radiative heat transportation by air at the fiber surface. The results show that, in the case of natural cooling, the thermal transportation is mainly limited by the heat transfer at the fiber surface. The air-clad impedes heat flow, especially when the width of the air clad is large. A narrower pump air-clad is advantageous, especially in actively cooled fiber lasers.

In 2004, the bar was raised in a collaborative work between Friedrich Schiller University Jena and Crystal Fibre A/S [28]. Their 7-cell fiber has an effective area of ~1000μm^2 and MFD of ~35μm (see Figure 5). Core diameter is ~40μm. Hole diameter d is 1.1μm and the pitch Λ is 12.3μm, giving a d/Λ=0.09. The fiber has a pump guide diameter of 170μm and a measured pump NA of 0.62 at 950nm. The pump absorption is ~13dB/m at 976nm. The pump air-clad is

http://dx.doi.org/10.5772/58958

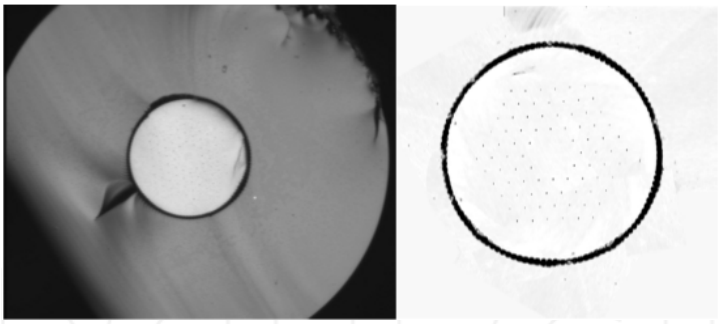

Figure 5. Microscope image of the air-clad ytterbium-doped single-mode PCF and close-up to the 40-μm core formed by seven missing air holes [28].

much narrower for more efficient heat diffusion. It is worth noting that the fiber is in the multimode regime for a 7-cell PCF (see Figure 5). This helps to ease bend loss in the weakly guided fiber.

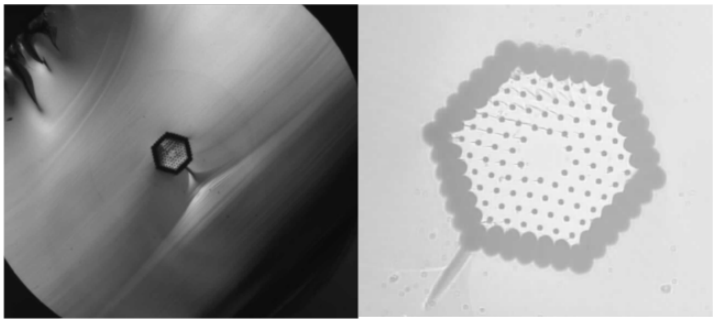

Figure 6. Microscope image of a rod-type photonic crystal fiber and close-up view of the inner cladding and core regions.

To further mitigate bend loss, a rod-type PCF was developed in 2005 [29] (see Figure 6). The rod had an outer diameter of 1.7mm so that it cannot be bent. A 48cm long length was used in the demonstration. The relative hole diameter was increased to d/Λ=0.33. This reduces bend sensitivity. This larger d/Λ in a 7-cell core PCF, however, puts this fiber firmly in the multimode regime (see Figure 2). The pump guide was reduced to a hexagon with flat-to-flat dimension of 117μm and corner-to-corner dimension of 141μm, similar to earlier fibers. The ytterbium doping level was also increased compared with earlier fibers. The increased doping level and reduced pump guide led to a high pump absorption of ~30dB/m at 976nm. The fiber was used to demonstrate power extraction of ~250W/m.

The rod-type PCF was further developed with the demonstration of a 19-cell PCF with a core diameter of 60μm, effective mode area of ~2000μm^2 and MFD of 75μm in 2006 [30] (see Figure

7). The fiber had a d/Λ=0.19, again firmly in the multimode regime (19-cell PCF not shown in Figure 2). The pump guide was 175μm in diameter. The pump air-clad had a web thickness of 400nm, which was 10μm long. The measured pump NA was 0.6 at 975nm, fairly close to the 0.67 NA predicted by the slab model (see Figure 3). The pump absorption is ~30dB/m at 976nm. The rod diameter is ~1.5mm. A 58cm long fiber was used to demonstrate 55W/m power extraction. In the same paper, a passive 100μm core fiber was also demonstrated. The 19-cell fiber had a d/Λ=0.2, again in the multimode regime. The effective mode area was ~4500μm^2 and MFD was ~75μm.

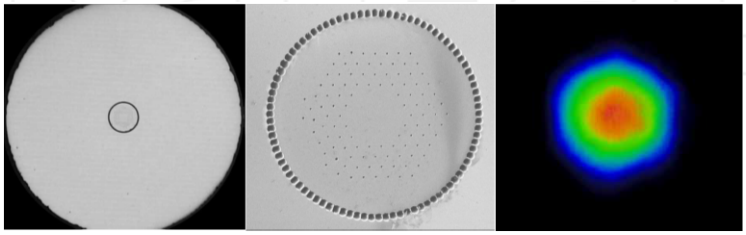

Figure 7. Microscope-image of the extended-mode-area rod-type photonic crystal fiber, SEM-picture of the micro-structured region and measured near-field intensity profile of the 60μm core fiber [30].

The demonstration of a 100μm active 19-cell PCF finally came in 2006 [6]. The pump guide had a diameter of 290μm. The rod diameter was 1.5mm. A 90cm long fiber was used to amplify 1ns pulses at 9.6kHz to record peak power of 4.5MW and pulse energy of 4.3mJ with M^2=1.3.

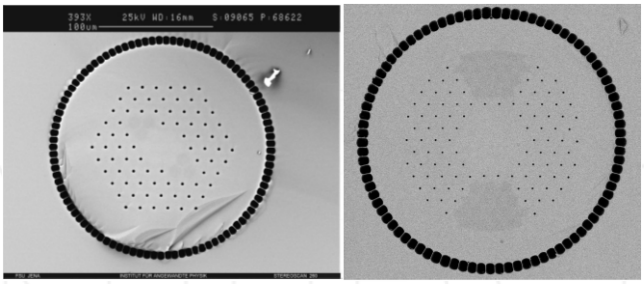

Figure 8. SEM image of the single polarization PCF with an effective area of ~700μm^2 [31] (left) and 2300μm^2 (right) [32].

Polarization-maintaining (PM) PCFs have also been developed by introducing stress elements. A PM 7-cell PCF with a mode area of ~700μm^2 was demonstrated in 2005 [31] (see left figure in Figure 8). The pitch Λ was 12.3μm with a d/Λ of 0.2. In the weakly guided PCFs, the polarization modes on slow and fast axis have different bend losses. This enables single-polarization operation where the polarization mode on the slow axis is still guided while polarization mode on the fast axis suffers high bend loss. Another single-polarization 19-cell

PCF was demonstrated in 2008 with a mode area of ~2300μm^2 (right figure in Figure 8) [32]. The corner-to-corner distance of the core was 70μm. The pitch Λ was 11μm with a d/Λ of 0.1.

3. Leakage channel fibers

A 2D micro-structured cladding, which is made possible by the stack-and-draw technique developed for photonic crystal fibers, enables new designs which do not possess the closed core-and-clad boundaries of conventional optical fibers. When a mode is guided in a conventional optical fiber, total internal reflection everywhere around the closed core-and-clad boundary, traps light entirely in the core, leading to zero waveguide loss. In designs with an open cladding, light can leak out, leading to finite waveguide loss associated with each mode. The waveguide loss is mode-dependent, providing opportunities for mode control by minimizing loss of the desired mode while maximizing loss of the unwanted modes. *Leakage channel fibers* (LCF) takes advantages of these new opportunities made possible by open cladding designs. A LCF can be precisely engineered to have high confinement loss for all higher order modes and low confinement loss for the fundamental mode and can, therefore, significantly extend the effective mode area of the fundamental mode. LCFs essentially exploit the increased ability of higher order modes to leak through small gaps in the cladding while maintaining good fundamental mode confinement.

3.1. Leakage channel fibers with air holes

The first LCF was demonstrated in 2005 [7]. It has a simple cladding design with air holes in the cladding [7]. The LCF is shown in in the left figure in Figure 9. The LCF had an outer diameter of ~270μm. The two smaller holes had a diameter of d=39.6μm and pitch Λ=51.2μm. The four larger holes had a diameter of d=46.0μm and pitch Λ=51.1μm. The passive LCF provided robust single-mode operation with a measured mode area of ~1417μm^2 (MFD=42.5μm). The most significant aspect of this work is that the LCF can be coiled down to 15cm with negligible loss penalty. This is a significant improvement over PCFs.

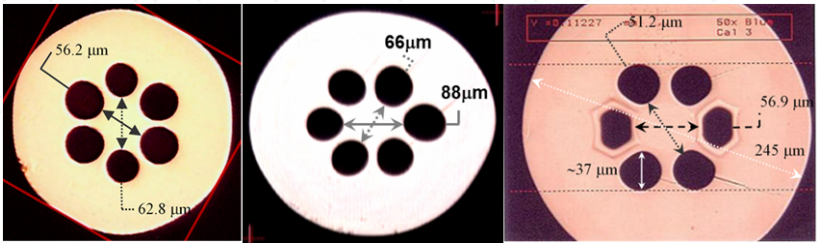

Figure 9. The LCF used in the first demonstration [7] (left), the first ytterbium-doped LCF (center) [33] and the first ytterbium-doped PM LCF (right) [34].

The first Ytterbium-doped LCF was demonstrated in 2006 [33] (see the middle figure in Figure 9). The fiber outer diameter was ~350μm and it was coated with a low index polymer to give a pump NA of 0.46. The average hole diameter was ~55μm and average pitch was ~67μm, giving an average d/Λ=0.82. The effective mode area was 3160μm^2 (MFD=63.4μm). Pump absorption was measured to be ~3.6dB/m at 976nm. Slope efficiency versus launched power was measured to be ~60% in a 5m long amplifier coiled at 40cm diameter. M^2 was measured to be ~1.3.

The first ytterbium-doped PM LCF was also demonstrated in 2006 [34] (see the right figure in Figure 9). A pair of boron-doped silica stress rods was used to replace two opposing air holes. The hole diameter was ~37μm. The effective mode area was ~1400μm^2 (MFD=42.2μm). The birefringence was measured to be ~2.1×10^{-4} over 1010-1080nm. The LCF had an outer diameter of ~245μm and was coated with a low index polymer to give a pump NA of ~0.46. The pump absorption was ~2.6dB/m at 976nm. Slope efficiency versus launched power was measured to be ~60%. M^2 was measured to be ~1.2. The PM LCF could be coiled to 12cm diameter with negligible bend loss.

3.2. All-glass leakage channel fibers

High refractive index contrast is not necessary for large core fiber designs. Low refractive index contrast is sufficient and often advantageous for further limiting higher order mode propagation. Fluorine-doped silica can be used to replace air holes in the LCFs described in the last section. The all-glass LCFs can provide much improved ease of fabrication and use, compared with fibers with air holes.

Despite the fact that air is a readily available ingredient, there are a number of drawbacks related to the use of air holes in fibers. The first one is the difficulty in precisely controlling the dimension of air holes in fiber fabrication. This is an intrinsic problem of a holey structure due to the air hole's tendency to collapse during fiber drawing. This is usually countered by a precise control of pressurization of the air holes, a process dependent on drawing conditions such as furnace temperature, feed rate, and drawing speed. When small air holes are desirable as in endless single-mode PCFs, higher pressure is required to maintain air hole dimensions due to the significantly increased tendency for the air holes to collapse by surface tension in this regime. This can make air hole dimensions to become highly sensitive to drawing conditions. This delicate balance of pressurization and collapse can lead to issues of controllability and repeatability in PCF fabrication. Air holes can also disturb smooth fracture wave propagation during fiber cleaving, leading to a poor cleaved surface due to the appearance of deep fractures behind the air holes, a problem often aggravated by large air holes and high cleaving tensions. In addition, air holes often have to be thermally sealed at the fiber ends to minimize environmental contamination. Mode distortion can occur from the air holes collapsing during splicing. This is especially true for large-mode-area fibers, which are much more susceptible to small perturbations.

A detailed analysis of all-glass LCFs was reported in [35]. For a LCF formed by one layer of features as shown in the inset of Figure 10, the core of diameter 2ϱ is formed by six features with diameter d and refractive index n_f. Center-to-center feature spacing is Λ. The refractive

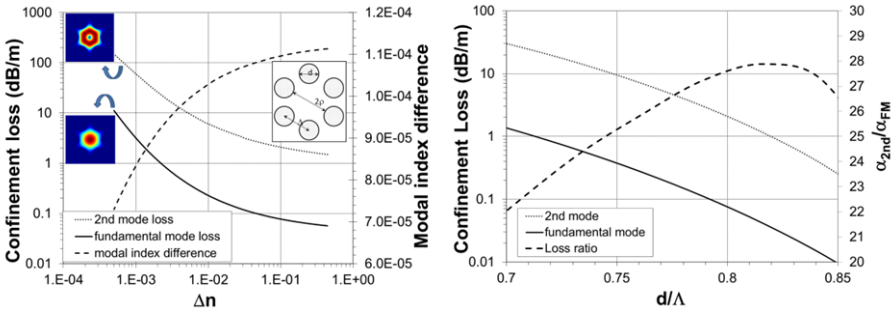

Figure 10. Effect of index contrast on confinement loss and modal index difference for one-cladding-layer LCFs with d/Λ=0.675 and 2ϱ=50μm (left) and effect of d/Λ on confinement loss and the loss ratio between the second-order mode and fundamental mode for LCFs with Δn=1.2×10^{-3} and 2ϱ=50μm (right) [35].

index of the background glass, usually silica, is n_b. The fiber was studied by a multipole mode solver for the effect of index contrast $\Delta n=n_b-n_f$. For the simulation in Figure 10, the following parameters were used: 2ϱ=50 μm, d/Λ=0.675, and n_b=1.444. The wavelength of the simulations was at 1.05μm. It can be seen from the left figure in Figure 10 that confinement loss for both fundamental, α_{FM}, and second-order modes, α_{2nd}, increases with a reduction of index contrast Δn, with the loss of the second-order mode, α_{2nd}, remaining over an order of magnitude higher than the loss of the fundamental mode, α_{FM}. The modal index difference, the difference between the effective mode indices of the fundamental and second modes, decreases toward low index with Δn by just ~40% over three orders of magnitude change in Δn.

The effect of normalized hole diameter d/Λ was also studied in [35] and is shown in the right figure in Figure 10 for confinement losses and the ratio of the second-mode loss to the fundamental-mode loss. The confinement loss for both the fundamental and second modes increases toward small d/Λ with the loss ratio changing very little over the entire range of d/Λ, from 22 to 28. The normalized hole diameter d/Λ is typically chosen to give an acceptable fundamental-mode loss. For LCFs with one layer of features as shown in Figure 10, the loss ratio of all-glass LCFs is very similar to that of an LCF with air holes. Slightly larger d/Λ is, however, required for achieving a similar confinement loss.

LCFs with two layers of features can be used to further improve the differential confinement loss between the fundamental and second-order modes at the expense of bending performance. Acceptable fundamental-mode loss at smaller feature sizes can be realized in LCFs with two layers of features, while leakage of higher order modes is substantially increased by a reduction of feature size despite the additional layer of features. Higher differential loss between modes can therefore be realized. Since bending loss of the fundamental mode is very strongly dependent on feature size, a reduction of feature size increases the bend loss of the fundamental mode in LCFs. An LCF with two layers of features was studied in [35] and the results are shown in Figure 11. Both the fundamental mode and second-order-mode loss shows the characteristic increase at small d/Λ, while the loss ratio α_{2nd}/α_{FM} is increased by over an order of magnitude compared to the one-layer designs in Figure 10. At d/Λ ≈ 0.548, the

fundamental-mode loss $\alpha_{FM} \approx 0.1$ dB/m, while the second-order-mode loss $\alpha_{2nd} \approx 48$ dB/m, a loss ratio α_{2nd}/α_{FM} of ~480. A very high loss ratio α_{2nd}/α_{FM} of ~700 is possible at d/Λ=0.62.

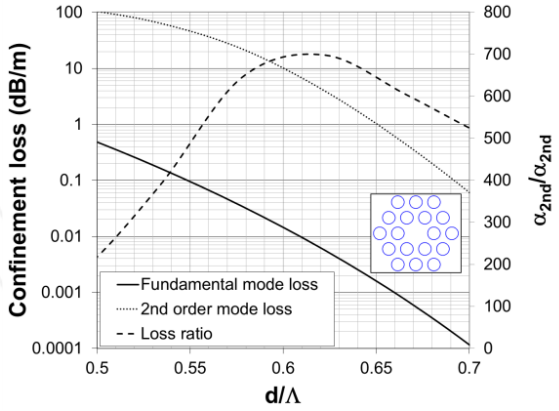

Figure 11. Effect of d/Λ on confinement loss and the loss ratio between the second-order mode and fundamental mode for an LCF with two layers of features, $\Delta n=1.2\times10^{-3}$ and $2\varrho=50\mu m$. [35].

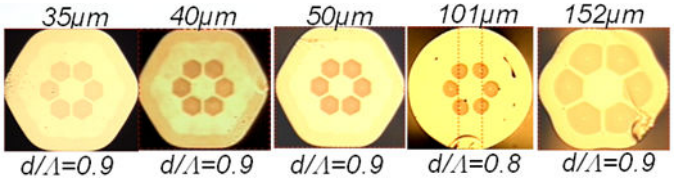

Figure 12. Some examples of fabricated all Glass LCFs. Core diameter is given above the fiber [35].

A wide range of all-glass LCFs were fabricated from core diameters from 35μm to well over 100μm [35] (see Figure 12). All fibers were made with silica glass as the background glass and slightly fluorine-doped silica glass as the cladding features and coated with standard coating with index of 1.54. The refractive index difference between the background and the low index feature wasΔ n=1.2×10^{-3}. LCFs with both circular and hexagonal features were fabricated and tested. The conditions for the fabrication of LCFs with hexagonal features also created LCFs with a rounded hexagonal outline. Such a shape is known to be preferred for the pump mode mixing in a double clad fiber where the pump light propagates in a much larger cladding guide. All the fabricated LCFs in Figure 12 operated in the fundamental mode with a varying degree of bend loss performance. In general, bend loss increases rapidly with core diameter increase (see Figure 13). This effect is fundamentally related to the fact that the ability of guided modes to navigate a bend is related to how rapidly a mode can change its spatial pattern without breaking up while propagating, i.e. maintain adiabatic transition. As the mode gets larger, this ability to change diminishes very quickly due to larger Rayleigh range.

http://dx.doi.org/10.5772/58958

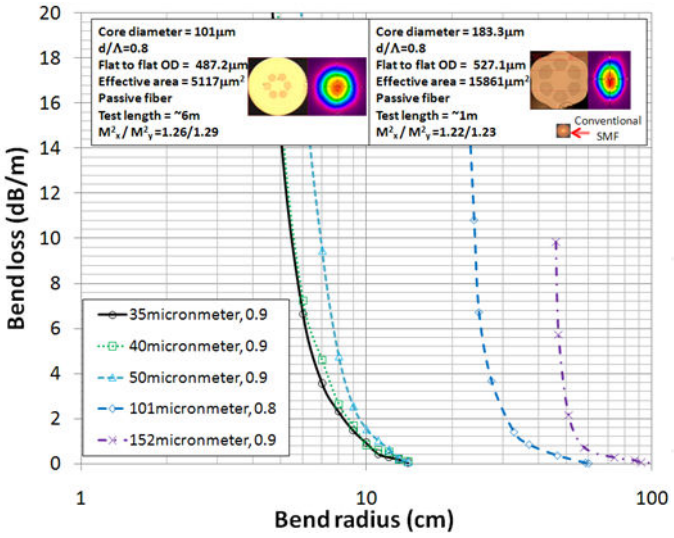

Figure 13. Cross section, measured mode and fiber details are given for the LCF with 101µm core, left inset, and the LCF with 183.3µm core, right inset. Measured bend loss for LCFs with various core diameters [36].

The LCF, shown on the top left inset in Figure 13, had 2ρ=101µm, and d/Λ=0.9. The effective mode area of the LCF was calculated to be 5117µm² (MFD=80.7µm). A length of the LCF ~6m long was loosely coiled in a 1m coil and the measured M^2 was M^2_x=1.26 and M^2_y=1.29. The LCF, shown on the top right inset, had 2ρ=183.3µm, and d/Λ=0.8. A conventional single mode optical fiber of the same scale is also shown for comparison. The effective mode area of this LCF was calculated to be 15861µm² (MFD=142.1µm), a record effective mode area for single-mode operation. The Measured M^2 of a 1m straight fiber is M^2_x=1.22 and M^2_y=1.23. Measured mode patterns at the output of the fibers are also shown in Figure 13.

3.3. Polarization maintaining all-glass leakage channel fibers

A PM all-glass LCF was first reported in [37] (see Figure 14). The passive all-glass PM LCF had a core diameter of 50µm. A high d/Λ=0.9 was used for a smaller critical bend radius. The LCF had a refractive index difference between the background and the low index feature of $\Delta n=1.2\times10^{-3}$. The low index features were made of slightly fluorine-doped silica. Two stress elements with a refractive index of ~13 × 10^{-3} below that of the background silica glass were used instead of the regular features on either sides of the core to provide birefringence. The fiber had an outer diameter of ~885µm and was coated with standard acrylic coating. The near field image measured with a single lens is shown in Figure 14(c) for the 1.8m long sample and in Figure 14(d) for the 30m sample. Due to the much higher d/Λ=0.9 used for this fiber, some bending was necessary for fundamental mode operation in a short length of this fiber. The output was robustly single mode in a 30m long sample of this passive LCF coiled in 40cm diameter coils (see Figure 14(d)). The critical bend radius for 1dB/m loss, expected to be ~11cm

by FEM simulation, matched very well to the 10.5cm measured. *Polarization extinction ratio* (PER) was characterized at the output of a 1.8m long sample to be >15dB over 1010-1100nm.

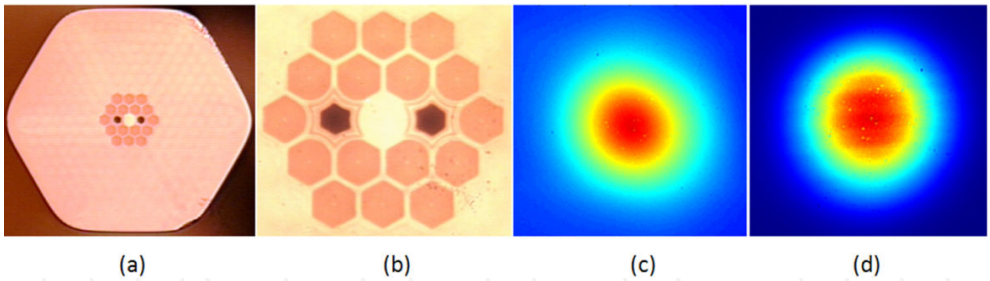

Figure 14. (a) Cross section of the passive PM LCF, (b) magnified cross section, (c) near field from the 1.8m long fiber in a 40cm-diameter coil, (d) near field from the 30m long fiber in a 40cm-diameter coil [37].

3.4. Characterization of mode losses in all-glass leaky channel fibers

Recently, fundamental and higher order mode losses have been characterized and compared to simulations based on the assumption of an infinite cladding [38]. A LCF with a ~50μm core diameter and a hexagonal cladding boundary (see Figure 15(a)) was spliced to a tunable source to ensure launch stability during the measurements. The passive LCF was coated with a low-index polymer to simulate a double-clad fiber with a pump NA of ~0.45. Power in various modes at the output was measured using the S^2 method [39]. The fiber was cut back several times to determine the propagation losses of various modes. The measurement was repeated at various coil diameters. The results are summarized in Figure 15(b) and show remarkable agreement between the measured and simulated losses of fundamental and higher-order modes. LP11 mode loss as high as ~20dB/m was measured, demonstrating the validity of the design. A similar LCF with a circular cladding boundary was also measured, showing significant less higher-order mode losses than those predicted by simulations. It is speculated that the coherent reflection at the circular cladding boundary played a significant role in enhancing the guidance of leaky higher-order modes in this case. It is, therefore, critical to have a non-circular cladding boundary to achieve the maximum possible higher-order mode losses.

3.5. Ytterbium-doped all-glass leakage channel fibers

An ytterbium-doped all-glass LCF with one layer of cladding features was also reported in [37]. The LCF was coated with a low index polymer, providing a pump NA of 0.45. This LCF had pump absorption of 11dB/m at ~976nm. The LCF also had 2ϱ=52.7μm and d/Λ=0.8. This gives a simulated effective area of 1548μm^2 at 1.05μm. The LCF has a rounded hexagonal shape and a flat-to-flat dimension of 254.2μm. The fiber was used to demonstrate amplification of 600ps pulses (with 600μJ pulse energy) to 1MW peak power.

http://dx.doi.org/10.5772/58958

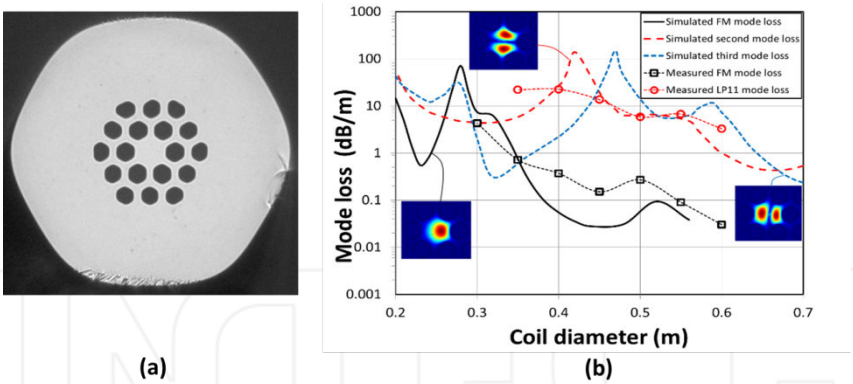

Figure 15. (a) The hexagonal LCF used in the measurement and (b) simulated and measured mode loss in the hexagonal Re-LCF [38].

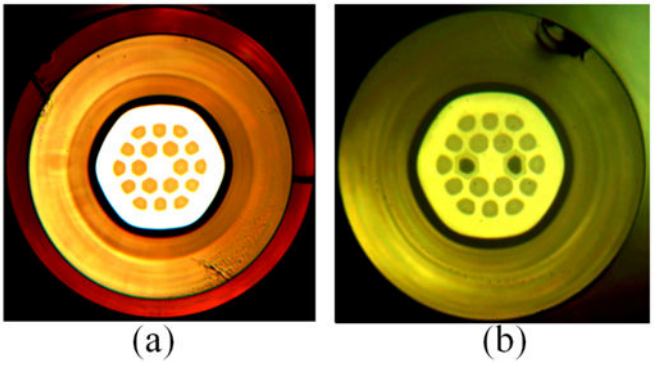

Figure 16. An all glass active LCF (left) and an all glass PM active LCF with highly fluorine-doped pump cladding (right) [37].

Ytterbium double-clad all-glass LCFs with highly fluorine-doped silica as pump cladding were also demonstrated (see Figure 16) [37]. All-glass LCFs have no polymer in the pump path and have independent control of the fiber outer diameters and pump cladding dimensions. This, therefore, enables designs with smaller pump guides for higher pump absorption and, at the same time, with larger fiber diameters to minimize micro and macro bending effects, a much desired feature for large core fibers where intermodal coupling could be an issue due much increased mode density. Stress rods can also be added for PM LCFs (see Figure 16).

The LCFs had a refractive index difference between the background and the low index feature of $\Delta n=1.2\times10^{-3}$. The non-PM LCF (see the left figure in Figure 16) had an inner layer $d/\Lambda=0.8$ and outer layer $d/\Lambda=0.7$. It had a 47μm core diameter, a rounded hexagon pump guide with a dimension of 238μm by 256μm, a pump NA of 0.28, pump absorption of ~12dB/m, and an outer diameter of ~538μm coated with standard high index coating, shown as the outermost

layer in Figure 16(a). A 3.5m fiber coiled in 53cm diameter was used to demonstrate a slope efficiency of 75% in an amplifier [37]. A single stage gain of 33dB was demonstrated using this fiber. It was also used to directly amplify 15ps pulses to a peak power of ~1MW.

The PM LCF (see Figure 16(b)) had a core diameter of 80μm and had a fluorine-doped pump cladding, providing a pump NA of ~0.28. Low index features with an inner layer d/Λ of 0.8 and an outer layer d/Λ of 0.7 were used. This active PM LCF had a pump guide diameter of ~400μm (flat-to-flat), a fiber outer diameter of ~835μm, and was coated with standard acrylic coating. Pump absorption was estimated to be ~12dB/m. The mode field diameter was measured to be ~62μm. The fiber was used as an amplifier in a single coil 76cm in diameter with a length of straight section at each end, demonstrating a slope efficiency of ~74% and a maximum single-path gain in excess of 30dB [37]. It demonstrated direct amplification of 14.2ps pulses to 190kW peak power with pulse energy of 2.74μJ and negligible SPM spectral broadening. M^2 was measured to be below 1.35 for the entire output power range.

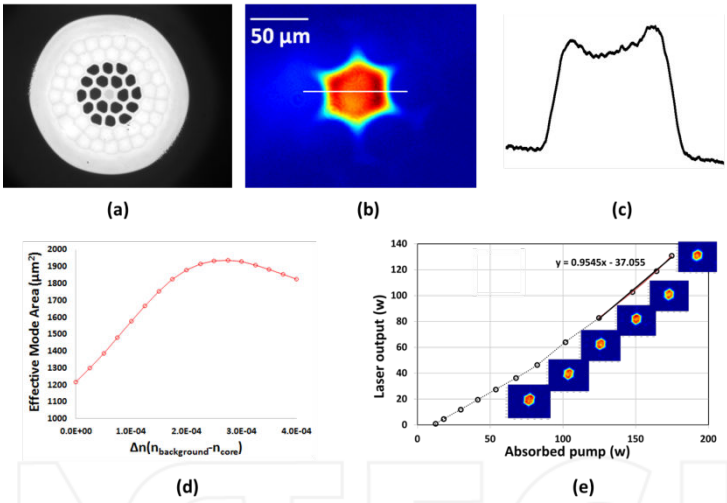

Figure 17. (a) The ytterbium-doped LCF with an index depression in the core center, (b) measured near field intensity of the guided mode, (c) measured mode intensity distribution, (d) simulated effective mode area versus the index depression, and (d) measured laser output and near field patters at various powers [40].

Recently, a flat-top mode has been demonstrated in an ytterbium-doped LCF with a ~50μm core by introducing an area ~30μm in diameter in the core center with a refractive index of ~2×10^{-4} lower than that of the background glass (Figure 17(a)) [40]. The flat-top mode (see Figure 17(b) and (c)) increased the effective mode area of the LCF from ~1200μm^2 to ~1900μm^2, a ~50% increase (see Figure 17(d)). The LCF also demonstrated near quantum-limited efficiency (see Figure 17(e)). Lasing wavelength was 1026nm and the pump was at 976nm.

http://dx.doi.org/10.5772/58958

4. Higher-order-mode fibers

The concept and demonstration of robust propagation of *higher-order-modes* (HOM) with large effective mode areas were first reported in 2006 [11]. It was argued that the stability of mode propagation in multimode fibers is critically dependent on the effective mode index difference between the propagating mode and its nearest neighbor anti-symmetric mode. This effective mode index difference is actually larger for the higher-order LP_{04}-LP_{07} modes than for the fundamental mode (see Figure 18). In addition, a *long period grating* (LPG), a fairly matured technology, can be used for broad band mode conversion to and from those higher-order LP0n modes.

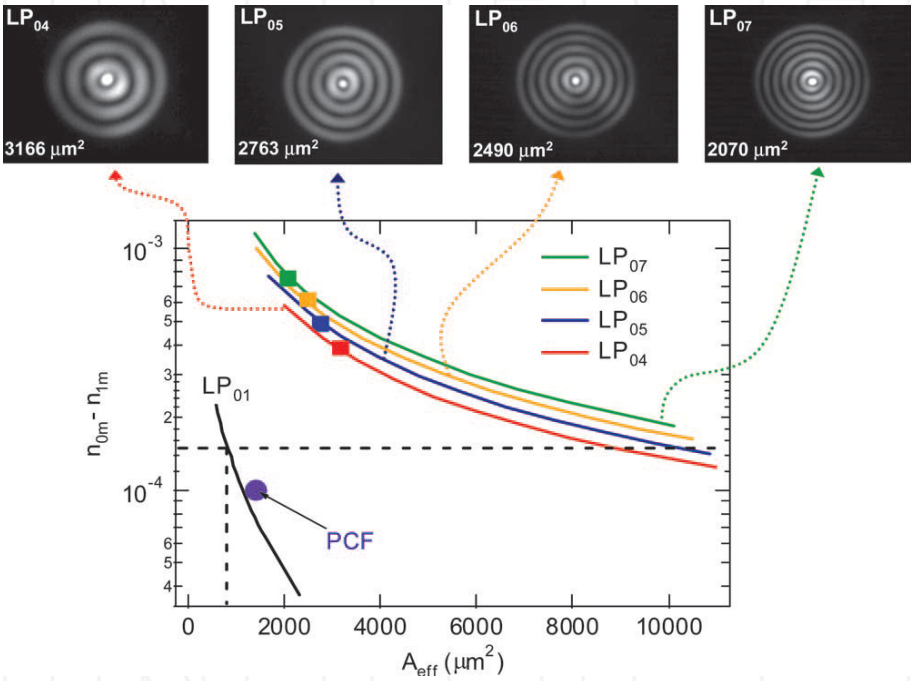

Figure 18. Effective index difference between nearest neighbor anti-symmetric mode versus A_{eff}. Top, near-field images of LPG-excited HOMs after >2m propagation with 7cm bend and with A_{eff} ranging from 2100 to 3200μm² [11].

Mode coupling first requires phase-matching. Perturbations on the fiber need to provide a vector which equals the difference in the propagation constants of the two modes involved. The larger the mode index difference between the two modes, the larger is the wave vector required for phase matching. A large wave vector implies high spatial frequency and small spatial period. For a mode index difference of 1.5×10^{-4}, the required spatial period of the perturbation at 1.55μm is ~10mm. Due to geometric constraints, the spatial frequency distribution of perturbations on fibers usually cuts off at a certain upper frequency limit. This would

minimize mode coupling between modes with larger effective mode index differences. The second requirement for mode coupling is that the overlap integral among the two modes and the perturbation needs to be non-zero. This requires the perturbation to break up the mode orthogonality. Although it was not explicitly spelled out in [11], it was assumed that the perturbations on fibers are mostly anti-symmetric. In this case, mode coupling dominates between LP0n and its anti-symmetric counterpart LP1n modes in optical fibers.

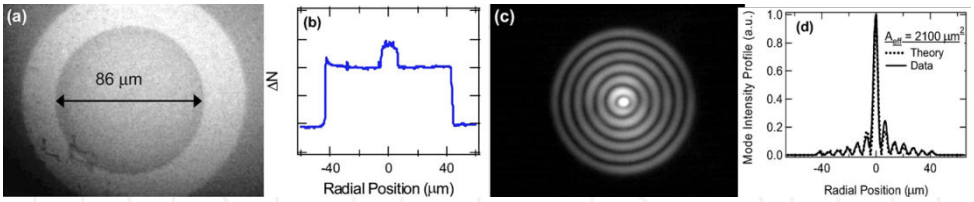

Figure 19. Characteristics of an HOM fiber. The horizontal and vertical scales of the images are identical. (a) Near-field image of a fiber facet, showing the 86μm inner cladding. (b) Refractive-index profile of the HOM fiber, with a core similar to an SMF with an 86μm inner cladding and a down-doped outer trench. (c) Near-field image of the LP_{07} mode at 1600 nm after 12m propagation with a 4.5cm radius bend. (d) Intensity line scan of (c) and theoretical profile: A_{eff}=~2100μm² [11].

The effective mode index difference for LP_{01}, LP_{04}, LP_{05}, LP_{06} and LP_{07} modes with their nearest neighbor anti-symmetric modes are shown versus effective mode area in Figure 18 [11]. The near-field images of the measured HOM modes are shown at the top of in Figure 18 and in Figure 19. It is clear that the effective mode index difference is significantly larger for the LP_{04}-LP_{07} modes than for the LP_{01} mode with the same effective mode area. The effective mode index difference also increases slightly for higher order LP_{0n} modes with the same effective mode area. For the same fiber, the effective mode area is actually larger for lower-mode-order LP_{0n} modes. The schematic of the proposed system is shown in Figure 20(a), where two identical LPGs are required for mode conversion from the LP_{01} mode to the LP_{07} mode and back to the LP_{01} mode. Robust propagation of the LP_{07} mode with an effective mode area of 2070μm² was demonstrated at 1600nm with the arrangement shown in Figure 19(c). The performance of the mode converter with high efficiency over broad bandwidth is shown in Figure 20(b). It was found that the LP_{07} mode suffered negligible bend loss at coil diameters down to 12cm. It was also found that modal stability increases with mode order. In a second paper [12], the effective mode areas of LP_{07} mode was simulated at various bend radii, showing stronger bend resistance than both LP_{03} and LP_{01} modes.

Recently, an erbium-doped HOM amplifier was demonstrated [41]. A small inner core was designed to have a LP_{01} mode MFD of 9μm, allowing for effective excitation of the LP_{01} mode when the HOM fiber was spliced to a single-mode fiber. Higher-order modes expanded to occupy the outer core. The LP_{010} mode had an effective mode area of 2700μm². Both the inner and the outer core were doped with erbium with absorption of ~30dB/m at 1530nm. The amplifier was both seeded at 1564nm and pumped at 1480nm in the LP_{010} mode. The pump was a Raman fiber laser.

http://dx.doi.org/10.5772/58958

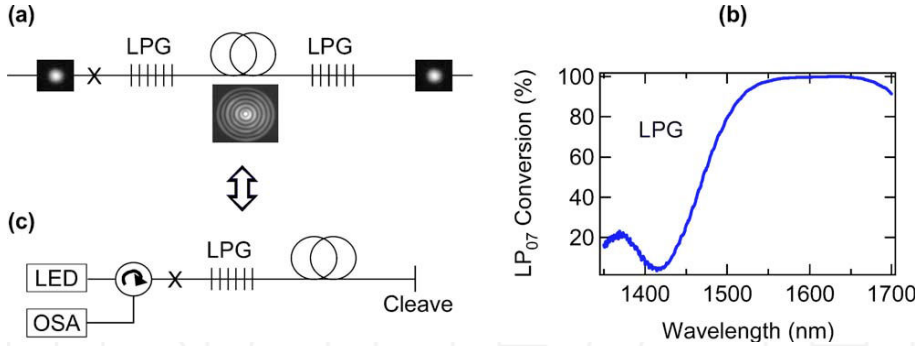

Figure 20. (a) Device schematic: light is coupled into and out of HOM with LPGs whose conversion efficiency being shown in (b). LPG with broadband coupling with efficiency >99% over 94 nm and with peak coupling efficiency as high as 99.93%. (c) Alternative schematic for characterizing HOM fibers: the cleave serves to fold the device propagation path so that the single LPG acts as both the input and the output LPG. X, splice; OSA, optical spectrum analyzer [11].

The difference in effective index between nearest neighbor anti-symmetric modes at λ=1564 nm as a function of their effective area is plotted as points in Figure 21(a) for the LP_{01} through LP_{010} modes in the fiber. The LP_{02} and LP_{03} modes have a large A_{eff}, but small mode spacing. As the mode order increases, mode spacing increases too, while A_{eff} decreases. Figure 21(b) shows the calculated intensity profiles at λ=1564nm for the LP_{01} and LP_{010} mode.

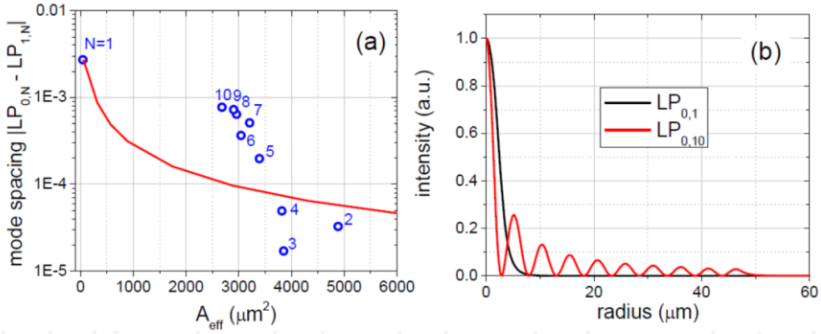

Figure 21. (a) Mode spacing as a function of effective area for the LP_{0n} modes in the HOM fiber (points) compared to a conventional LP_{01} step-index fiber with V=5 (solid curve). (b) Intensity profiles of the LP_{01} and LP_{010} modes. These calculations were done at a wavelength of 1564 nm.

A narrow line width, external cavity laser was amplified to 50mW and combined with the high-power, single mode Raman fiber laser at 1480 nm in a single-mode pump/signal combiner. The output of the pump/signal combiner was fusion-spliced to the HOM fiber. The length of the amplifier fiber after the LPG was 2.68 m. The measured slope efficiency at 1564nm was 43.2%. Over 20dB of gain was demonstrated by the amplifier.

5. Chrially-coupled core fibers

A C*hirally-coupled-core* (CCC) fiber was first reported in 2007 [9]. The fiber had a large central core and a smaller side core wound around the central core in a helical fashion (Figure 22). The preform had two parallel cores and the fiber was spun during the draw to form the helical side core. In this first report, the central core had a diameter of 35μm and a NA of 0.07. The side core had a diameter of 12μm and NA of 0.09. Edge-to-edge core separation was 2μm. The helical pitch was 6.2mm. The fiber was measured to be single-mode at 1550nm over a short length of 25cm. It was multimode below 1500nm. The simulation predicted LP_{01} mode loss to be 0.3dB/m and all HOM loss to be >130dB/m for λ>1550nm. The fiber was also confirmed to be polarization-maintaining.

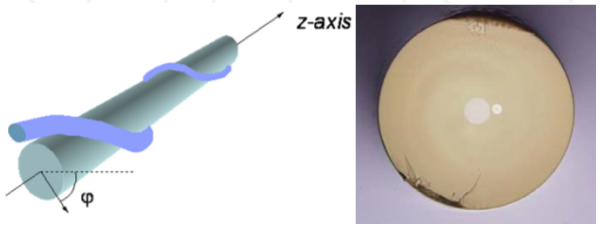

Figure 22. Structure of Chirally-coupled-core fiber [9].

The propagation of modes in the central core was affected by the coupling of modes between the central and side cores. The fiber was designed to operate where there was no fundamental mode coupling with modes in the side core. Higher-order modes in the central core were, however, coupled with the side core modes at the operating wavelength. The modes in the side core had high loss due to the tight bend from the helical arrangement. This led to high loss for the higher-order modes in the central core which were coupled to modes in the side core.

An ytterbium-doped CCC fiber was demonstrated in a subsequent paper [10]. The ytterbium-doped central core had a 33μm diameter and 0.06 NA. The undoped side core had a 16μm diameter and 0.1 NA. The helical pitch was 7.4mm and the edge-to-edge core separation was 4μm. The low index coating provided a pump NA of 0.47. The pump guide had a 250μm diameter. The measured pump absorption was 2dB/m at 915nm. The fiber demonstrated 75% slope efficiency at 1066nm in a laser configuration.

In a more recent paper [42], a more detailed theoretical analysis of quasi-phase-matching (QPM) assisted by spin and orbital angular momentum was given. For two LP modes LP_{l1m1} and LP_{l2m2}, QPM is achieved when

$$\beta_{l1m1} - \beta_{l2m2}\sqrt{1 + K^2R^2} - \Delta mK = 0 \tag{2}$$

http://dx.doi.org/10.5772/58958

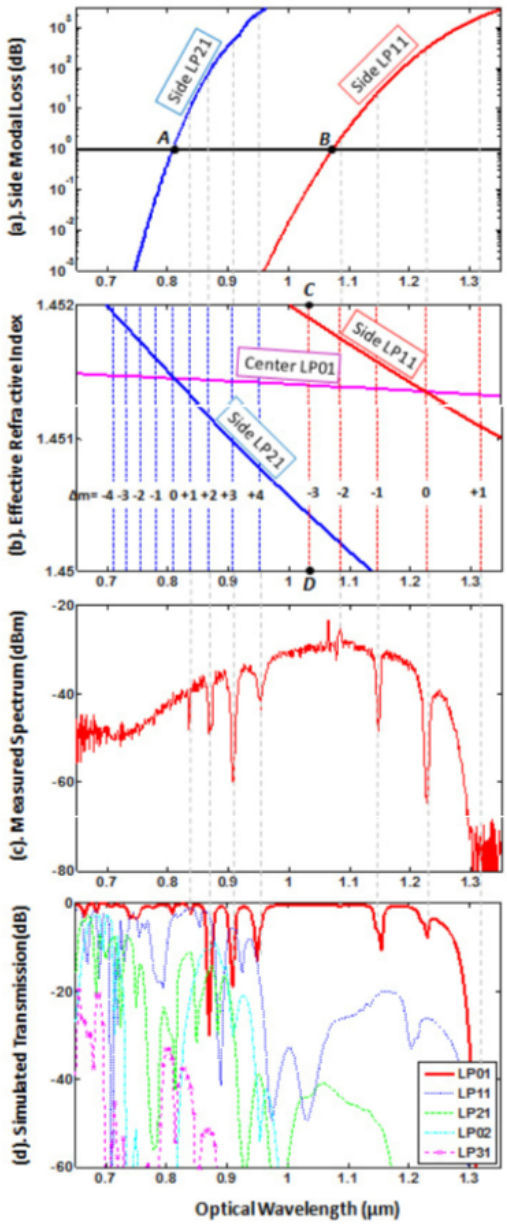

Figure 23. Calculation and measurement of quasi-phase-matching (QPM) for 1.5m-long CCC fiber sample. (a) Calculated loss for side-core LP_{11} and LP_{21} modes as a function of wavelength (top). (b) Calculated refractive indices of interacting modes and calculated QPM resonance positions. (c) Transmission of central core. (d) Simulated transmission of central core.

where β_{l1m1} and β_{l1m2} are the respective propagation constants of the two modes; $K=2\pi/\Lambda$; and Λ is helical pitch. $\Delta m=\Delta l+\Delta s$; $\Delta l=\pm l1\pm l2$; Δs=-2,-1, 0, 1, 2. The loss versus wavelength for the LP_{11} and LP_{21} modes in the side core is plotted in Figure 23(a) showing high loss for these modes in certain wavelength regimes. The mode indices of the LP_{11} and LP_{21} modes of the side core and LP_{01} mode of the central core are plotted in Figure 23(b). It can be seen clearly that the LP_{11} mode and LP_{21} modes of the side core naturally phase-match to the LP_{01} mode of the central core at ~1.22μm and ~0.81μm respectively. The QPM by angular momentum from the helical side core extends the phase matching to a number of other wavelengths determined by equation 2. These phase matching wavelengths are plotted in Figure 23(b) as red dotted vertical lines for the LP_{11} mode of the side core and the LP_{01} mode of central core coupling and blue dotted vertical lines for the LP_{21} mode of side core and LP_{01} mode of central core coupling. The measured transmission of the central core is plotted in Figure 23(c). The analysis of the CCC fiber can be simplified significantly in a helical coordination. The Maxwell equations keep the same form in the new coordination system, but the tenor form of permittivity and permeability needs to be transformed [42]. The resulting tenor does not have any z-dependence, which significantly simplifies the analysis. The simulated loss of various modes is shown in Figure 23(d), demonstrating that the narrow peaks in the transmission arise from coupling between the LP_{01} mode in the central core and the LP_{11} and LP_{21} modes in the side core.

The high loss of the LP_{01} mode in the central core at λ>1.3μm was not explained in the paper. It may be due to the angular momentum assisted coupling between LP_{01} mode in the central core and LP_{01} mode in the side core. This long wavelength cut-off has been used for the suppression of stimulated Raman scattering in fibers [43].

The higher loss for the higher-order-modes in the central core between 1-1.1μm in Figure 23(d) was not clearly explained either. For the LP_{11} mode in the central core, one possible reason for its high loss is coupling to LP_{21} mode of the side core through angular momentum-assisted QPM. Recently, a 60μm core CCC fiber was also demonstrated [44].

6. Photonic bandgap fibers

The guidance of light in a defect in a photonic bandgap fiber is based on fundamentally different principles compared to conventional optical fibers. In a conventional optical fiber, the core has a higher refractive index than that of the cladding. Light is guided through total internal reflection at the core-and-cladding boundary. In a photonic bandgap fiber, the photonic crystal cladding is designed to have photonic bandgaps, where there is an absence of modes propagating in the direction parallel to the fiber axis. Once a defect core is created within such a photonic crystal cladding, light is trapped to propagate only in modes of the defect core as it is forbidden to propagate in the cladding. This leads to significantly lower waveguide loss for the modes in the defect core within the cladding photonic bandgaps. This waveguide loss becomes zero when the photonic crystal cladding is infinite, but there is always a finite loss for practical fibers with finite cladding. This waveguide loss can, however, be significantly lowered by increasing the number of cladding layers.

http://dx.doi.org/10.5772/58958

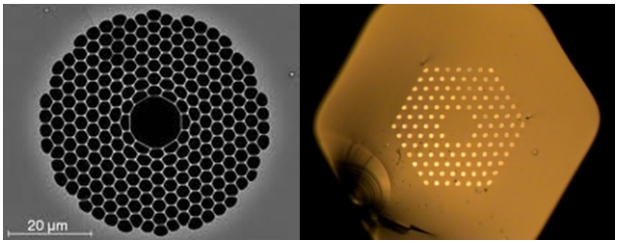

Figure 24. Images of a hollow-core photonic bandgap fiber (left) and an all-solid photonic bandgap fiber (right).

One unique feature of photonic bandgap fibers is that the defect core always has a lower refractive index than that of the higher refractive index material in the cladding. This leads to the possibility of hollow-core photonic bandgap fibers (see Figure 24, left), where light is guided mostly in the air in the hollow-core of the fiber. These fibers have extremely low nonlinearities and are well suited for high power laser delivery. The second type of photonic bandgap fibers are made entirely of glass (see Figure 24, right). These all-solid photonic bandgap fibers have a cladding which consists of a background glass and nodes of slightly higher refractive index. The much lower refractive index contrast (typically just a few percent) in the photonic crystal cladding of the all-solid photonic bandgap fibers still allows photonic bandgaps for paraxial propagation. Another important feature of photonic bandgap fibers is that their transmission is highly wavelength-dependent, i.e. low loss is possible only within the photonic bandgaps of the photonic crystal cladding. This distributive spectral filtering along a fiber can be very useful for range of potential applications including use in fiber lasers at low gain regimes to minimize gain competition, the suppression of stimulated Raman scattering, etc.

Birks et al. clearly explained the origin of the modes in the photonic crystal cladding of an all-solid photonic bandgap fiber in [45]. The density of states (DOS) of modes in the photonic crystal cladding is represented by the shades of grey in Figure 25 [45]. The refractive index of the background glass is represented by the black horizontal line. It is the cut-off line for the modes guided in the cladding nodes. The bandgap regime is represented by the red area. The fundamental mode of the defect core is illustrated by the yellow lines. The modes in the photonic crystal cladding clearly originate from the guided modes of the nodes, which are also labeled at the top of the figure. Above the background index, the modes form relatively narrow bands. Below the background index, the bands of modes significantly broaden, due to strong coupling among nodes as a result of light becoming more spread into the background glass below cut-off. The guidance property can be easily understood once it is recognized that there is a simple analogue to conventional optical fibers [46]. The core index is simply the index of the background glass and the equivalent cladding index is the upper boundary of the photonic bandgap. The effective index of the modes in the defect core (see yellow lines in Figure 25) falls between the core and cladding indices as in conventional optical fibers.

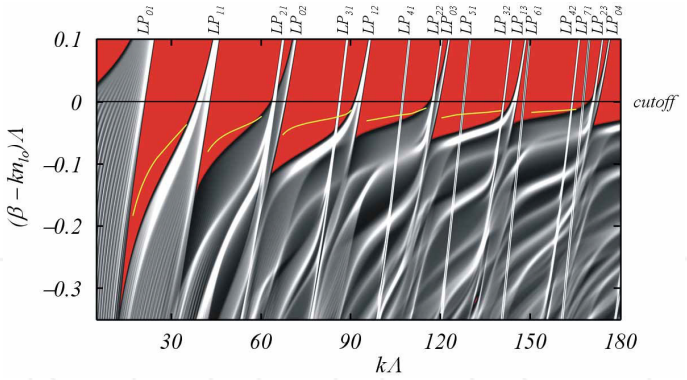

Figure 25. Plots of band structure for an example bandgap fiber. The bandgaps are shown in red. The node modes from which the bands arise are labeled along the top. Density of states (DOS) calculated using the plane-wave method, with light grey corresponding to high DOS. The yellow curve is the "fundamental" core-guided mode [45].

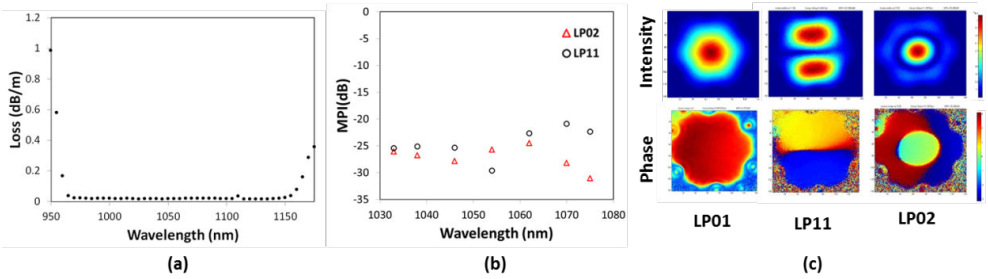

Figure 26. (a) Transmission of the 55μm core all-solid photonic bandgap fiber, (b) measured HOM contents with a S^2 method in a 5m fiber coiled at 70cm diameter, and (c) measured mode images [51].

One interesting application of ytterbium-doped all-solid photonic bandgap fibers is for the lasing of ytterbium at the long wavelength regime of 1150-1200nm [47]. It is normally difficult to lase in ytterbium-doped fibers at these extremely long wavelengths due to strong gain competition from the short wavelength regime of 1030-1070nm. The distributive spectral filtering in a photonic bandgap fiber can be used to minimize gain at short wavelengths, leading to efficient high power lasers in the extremely long wavelength regime.

In all-solid photonic bandgap fibers, a mode is guided only when it falls within the photonic bandgap of the cladding lattice. Guidance can therefore be highly mode-dependent. This provides great potential for creating designs that support only the fundamental mode, i.e. selective mode guidance. Mode area scaling to 20μm mode field diameter using all-solid photonic bandgap fibers was reported in [48]. Recently, all-solid photonic bandgap fibers with up to ~700μm^2 effective mode area have been demonstrated operating in the first bandgap [49, 50]. More recently, a fiber with a core diameter of ~55μm and an effective mode area of

http://dx.doi.org/10.5772/58958

920μm² at coil diameter of 50cm was demonstrated (see right figure in Figure 24). The fiber operates in the third bandgap with transmission shown in Figure 24(6). At 70cm coil diameter, a 5m fiber showed HOM contents below 25dB (see Figure 26(b) and (c)). At the design coil diameter of 50cm, HOM content was below-30dB [51].

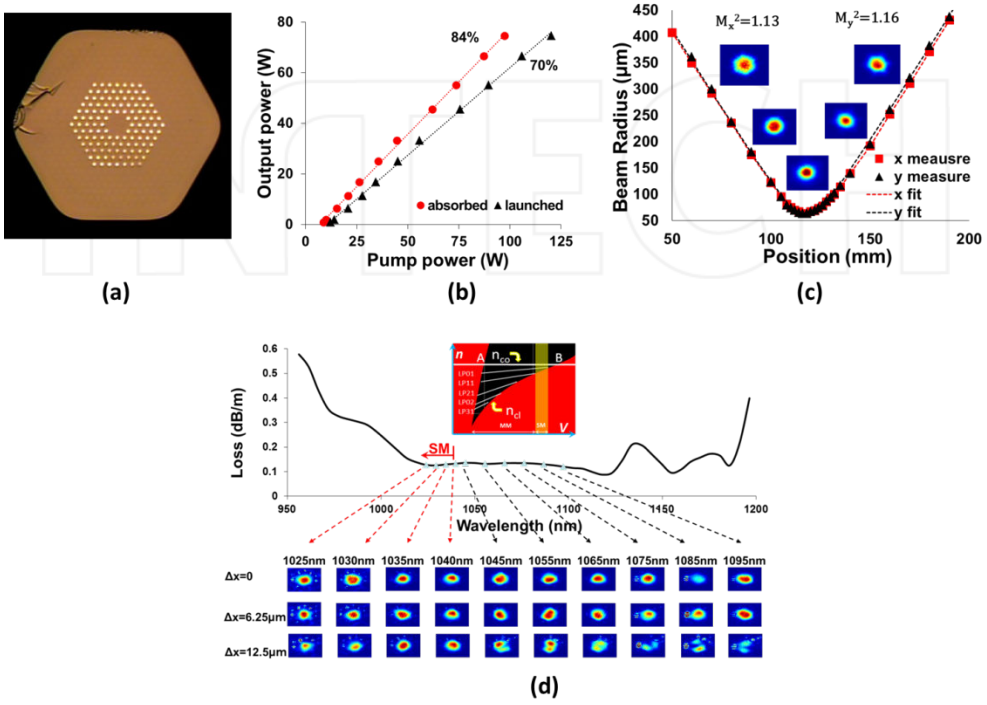

Figure 27. (a) Ytterbium-doped ~50μm core all-solid photonic bandgap fiber, (b) Laser efficiency, (c) M^2 measurement and (d) mode at various wavelengths across the bandgap [52].

Recently, an ytterbium-doped all-solid photonic bandgap fiber with ~50μm core diameter has also been demonstrated (Figure 27(a)) [52]. The fiber demonstrated high efficiency and excellent mode quality (see Figure 27(b) and (c)). The fiber also demonstrated robust single-mode behavior near the short wavelength edge of the bandgap by monitoring the output when moving away from the optimum launch condition (see Figure 27(d)). This is exactly expected from the dispersive nature of the photonic bandgap cladding.

7. Conclusions

In this chapter, we have briefly introduced a number of emerging fiber technologies for mode area scaling for fiber lasers. These new technologies are critical for the further power scaling

of fiber lasers. The basic principles of these technologies were introduced and the latest developments were discussed. This is still a very active area of research. With further development, there is great potential to significantly improve throughput and expand the capabilities of fiber lasers for use in manufacturing, as well as to meet future defense needs.

Author details

Liang Dong*

Department of Electrical and Computer Engineering, University of Clemson, Clemson, SC, USA

References

[1] D. Taverner, D.J. Richardson, L. Dong, J.E. Caplen, K. Williams, R.V. Penty, "158μJ pulses from a single transverse mode, large mode-area EDFA", Optics Letters, 22, 378-380 (1997).

[2] H.L. Offerhaus, N.G. Broderick, D.J. Richardson, R. Sammut, J. Caplen and L. Dong, "High-energy single-transverse-mode Q-switched fiber laser based on a multimode large-mode-area erbium-doped fiber", Optics Letters, 23, 1683-1685 (1998).

[3] C. Knight, T. A. Birks, P. St. J. Russell, and D. M. Atkin, "All-silica single-mode optical fiber with photonic crystal cladding," Opt. Lett. 21, 1547-1549 (1996).

[4] T.A. Birks, J.C. Knight and P.St.J. Russell, "Endlessly single-mode photonic crystal fiber," Opt Lett. 22 961-963 (1997).

[5] J.C. Knight, T.A. Birks, R.F. Cregan, P.St.J. Russell and J.P. de Sandro, "Large mode area photonic crystal fibre," Elect. Lett. 34, 1347-1348 (1998).

[6] C.D. Brooks and F. Teodoro, "Multi-MW peak-power, single-transverse-mode operation of a 100μm core diameter, Yb-doped rodlike photonic crystal fiber amplifier," Appl. Phys. 89, 111119 (2006).

[7] W.S. Wong, X. Peng, J.M. McLaughlin and L. Dong, "Breaking the limit of maximum effective area for robust single-mode propagation in optical fibers", Optics Letters, 30, 2855-2857 (2005).

[8] L. Dong, X. Peng and J. Li, "Leakage channel optical fibers with large effective area", Journal of Optical Society of America B, 24, 1689-1697 (2007).

[9] C.H. Liu, G. Chang, N. Litchinitser, A. Galvanauskas, D. Guertin, N. Jacobson and K. Tankala, "Effective single-mode chirally-coupled core fiber," Advanced Solid State Photonics, paper ME2, 2007.

[10] A. Galvanauskas, M.C. Swan, and C.H. Liu, "Effectively-Single-Mode Large Core Passive and Active Fibers with Chirally-Coupled-Core structures," Conference on Lasers and Electro-Optics, paper CMB1, 2008.

[11] S. Ramachandran, J. W. Nicholson, S. Ghalmi, M. F. Yan, P. Wisk, E. Monberg, and F. V. Dimarcello, "Light propagation with ultralarge modal areas in optical fibers," Opt. Lett. 31, 1797-1799 (2006).

[12] J.M. Fini and S. Ramachandran, "Natural bend-distortion immunity of higher-order-mode large-mode-area fibers" Opt. Lett. 32, 748-750 (2007).

[13] M. Koshiba and K. Saitoh, "Applicability of classical optical fiber theories to holey fibers," Opt. Lett. 29, 1739-1740 (2004).

[14] K. Saitoh, Y. Tsuchida, and M. Koshiba, "Endlessly single-mode holey fibers: the influence of core design," Opt. Express 13, 10833-10839 (2005).

[15] B. T. Kuhlmey, R. C. Mcphedran, and C. M. de sterke, "Modal cutoff in microstructured optical fiber," Opt. Lett. 27, 1684-1686 (2002).

[16] J. Zhou, K. Tajima, K. Nakajima, K. Kurokawa, C. Fukai, T. Matsui, and I. Sankawa, "Progress on low loss photonic crystal fibers," Optical Fiber Technology 11 101–110 (2005).

[17] T. P. White, B. T. Kulmey, R. C. McPhedran, D. Maystre, G. Renversez, C. Martijn de Sterke, and L. C. Botten, "Multipole method for microstructured optical fibers. I. Formulation," J. Opt. Soc. Am. B 19, 2322-2330 (2002).

[18] B.T. Kuhlmey, T.P. White, G. Renversez, D. Maystre, L.C. Botten, C. M. de Sterke, and R. C. McPhedran, "Multipole method for microstructured optical fibers. II. Implementation and results," J. Opt. Soc. Am. B 19, 2331-2340 (2002).

[19] W.J. Wadsworth, J.C. Knight and P.St.J. Russell, "Large mode area photonic crystal fiber laser," Conference on Lasers and Electro-Optics, CWC1, 2001.

[20] W.J. Wadsworth, R.M. Percival, G. Bouwmans, J.C. Knight and P.St.J. Russell, "High power air-clad area photonic crystal fiber laser," Opt. Express 11, 48-53 (2003).

[21] D.J. DiGiovanni and R.S. Windeler: "Article comprising an airclad optical fiber," US patent 5907652 (1999).

[22] V. A. Kozlov, J. Hernández-Cordero, R. L. Shubochkin, A. L. G. Carter, and T. F. Morse, "Silica–Air Double-Clad Optical Fiber," IEEE Photonics Technology Letters 12, 1007-1009 (2000).

[23] J.K. Sahu, C.C. Renaud, K. Furusawa, R. Selvas, J.A. Alvarez-Chavez, D.J. Richardson and J. Nilsson, "Jacketed air-clad cladding pumped ytterbium-doped fibre laser with wide turning range," Elect. Lett. 37, 1116-1117 (2001).

[24] K. Furusawa, A. Malinowski, J. H. V. Price, T. M. Monro, J. K. Sahu, J. Nilsson and D. J. Richardson, "Cladding pumped Ytterbium-doped fiber laser with holey inner and outer cladding," Opt. Express 9, 714-720 (2001).

[25] W.J. Wadsworth, R.M. Percival, G. Bouwmans, J.C. Knight, T.A. Birks, T.D. Hedley, and P.St.J. Russell, "Very high numerical aperture fibers," IEEE Photonic Technology Letters 16, 843-845 (2004).

[26] J. Limpert, T. Schreiber, S. Nolte, H. Zellmer, A. Tünnermann, R. Iliew, F. Lederer, J. Broeng, G. Vienne, A. Petersson, and C. Jakobsen, "High-power air-clad large-mode-area photonic crystal fiber laser," Opt. Express 11, 818-823 (2003).

[27] J. Limpert, T. Schreiber, A. Liem, S. Nolte, H. Zellmer, T. Peschel, V. Guyenot, and A. Tünnermann, "Thermo-optical properties of air-clad photonic crystal fiber lasers in high power operation," Opt. Express 11, 2982-2990 (2003).

[28] J. Limpert, A. Liem, M. Reich, T. Schreiber, S. Nolte, H. Zellmer, A. Tünnermann, J. Broeng, A. Petersson, and C. Jakobsen, "Low-nonlinearity single-transverse-mode ytterbium-doped photonic crystal fiber amplifier," Opt. Express 12, 1313-1319 (2004).

[29] J. Limpert, N. Deguil-Robin, I. Manek-Hönninger, F. Salin, F. Röser, A. Liem, T. Schreiber, S. Nolte, H. Zellmer, A. Tünnermann, J. Broeng, A. Petersson, and C. Jakobsen, "High-power rod-type photonic crystal fiber laser," Opt. Express 13, 1055-1058 (2005).

[30] J. Limpert, O. Schmidt, J. Rothhardt, F. Röser, T. Schreiber, and A. Tünnermann, S. Ermeneux, P. Yvernault, and F. Salin, "Extended single-mode photonic crystal fiber lasers," Opt. Express 14, 2715-2720 (2006).

[31] T. Schreiber, F. Röser, O. Schmidt, J. Limpert, R. Iliew, F. Lederer, A. Petersson, C. Jacobsen, K. P. Hansen, J. Broeng, and A. Tünnermann, "Stress-induced single-polarization single-transverse mode photonic crystal fiber with low nonlinearity," Opt. Express 13, 7622-7630 (2005).

[32] O. Schmidt, J. Rothhardt, T. Eidam, F. Röser, J. Limpert, A. Tünnermann, K.P. Hansen, C. Jakobsen, and J. Broeng, "Single-polarization ultra-large-mode-area Yb-doped photonic crystal fiber," Opt. Express 16, 3918-3923 (2008).

[33] L. Dong, J. Li and X. Peng, "Bend resistant fundamental mode operation in ytterbium-doped leakage channel fibers with effective areas up to 3160μm^2", Optics Express, 14, 11512-11519 (2006).

[34] X. Peng and L. Dong, "Fundamental mode operation in polarization-maintaining ytterbium-doped fiber with an effective area of 1400μm^2", Optics Letters, 32, 358-360 (2006).

[35] L. Dong, T.W. Wu, H.A. McKay, L. Fu, J. Li and H.G. Winful, " All-glass large core leakage channel fibers, " IEEE Journal of Selected Topics in Quantum Electronics, 15, invited paper, 47-53(2009).

[36] L. Dong, H.A. Mckay, A. Marcinkevicius, L. Fu, J. Li, B.K. Thomas, and M.E. Fermann, " Extending Effective Area of Fundamental Mode in Optical Fibers, " IEEE Journal of Lightwave Technology, 27, invited paper, 1565-1570(2009).

[37] L. Dong, H.A. Mckay, L. Fu, M. Ohta, A. Marcinkevicius, S. Suzuki, and M.E. Fermann, "Ytterbium-doped all glass leakage channel fibers with highly fluorine-doped silica pump cladding, " Optical Express, 17, 8962-8969(2009).

[38] G. Gu, F. Kong, T.W. Hawkins, P. Foy, K. Wei, B. Samson, and L. Dong, "Impact of fiber outer boundaries on leaky mode losses in leakage channel fibers," Optics Express 21, 24039-24048 (2013).

[39] J. W. Nicholson, A. D. Yablon, S. Ramachandran, and S. Ghalmi, "Spatially and spectrally resolved imaging of modal contents in large-mode-area fibers," Opt. Express 16, 7233-7243(2008).

[40] F. Kong, G. Gu, T.W. Hawkins, J. Parsons, M. Jones, C. Dunn, M.T. Kalichevsky-Dong, K. Wei, B. Samson, and L. Dong, "Flat-top mode from a 50 μm-core Yb-doped leakage channel fiber," Optics Express 21, 32371-32376 (2013).

[41] J.W. Nicholson, J.M. Fini, A.M. DeSantolo, E. Monberg, F. DiMarcello, J. Fleming, C. Headley, D.J. DiGiovanni, S. Ghalmi, and S. Ramachandran, "A higher-order-mode Erbium-doped-fiber amplifier," Opt. Express 18, 17651-17657 (2010).

[42] X. Ma, C.H. Liu, G. Chang, and A. Galvanauskas, "Angular-momentum coupled optical waves in chirally-coupled-core fibers," Opt. Express 19, 26515-26528 (2011).

[43] X. Ma, I,N Hu, and A. Galvanauskas, "Propagation-length independent SRS threshold in chirally-coupled-core fibers," Opt. Express 19, 22575-22581 (2011).

[44] X. Ma, A. Kaplan, and A. Galvanauskas, "Experimental characterization of robust single-mode operation of 50μm and 60μm core chirally coupled core optical fibers," PhotonicsWest, paper 8237-59, 2012.

[45] T. A. Birks, G. J. Pearce, D. M. Bird, "Approximate band structure calculation for photonic bandgap fibers," Opt. Express 14, 9483-9490 (2006).

[46] M.J.F. Digonnet, H.K. Kim, G.S. Kino, and S. Fan, "Understanding Air-Core Photonic-Bandgap Fibers: Analogy to Conventional Fibers," Journal of Lightwave Technology 23, 4146-4177 (2005).

[47] A. Shirakawa, H. Maruyama, K. Ueda, C. B. Olausson, J. K. Lyngsø, and J. Broeng, "High-power Yb-doped photonic bandgap fiber amplifier at 1150-1200 nm," Opt. Express 17(2), 447–454 (2009).

[48] O. N. Egorova, S. L. Semjonov, A. F. Kosolapov, A. N. Denisov, A. D. Pryamikov, D. A. Gaponov, A. S. Biriukov, E. M. Dianov, M. Y. Salganskii, V. F. Khopin, M. V.

Yashkov, A. N. Gurianov, and D. V. Kuksenkov, "Single-mode all-silica photonic bandgap fiber with 20-micron mode-field diameter," Opt. Express 16, 11735–11740 (2008).

[49] M. Kashiwagi, K. Saitoh, K. Takenaga, S. Tanigawa, S. Matsuo, and M. Fujimaki, "Low bending loss and effectively single-mode all-solid photonic bandgap fiber with an effective area of 650μm^2.," Opt. Lett. 37, 1292–1294 (2012).

[50] M. Kashiwagi, K. Saitoh, K. Takenaga, S. Tanigawa, S. Matsuo, and M. Fujimaki, "Effectively single-mode allsolid photonic bandgap fiber with large effective area and low bending loss for compact high-power all-fiber lasers," Opt. Express 20, 15061–15070 (2012).

[51] F. Kong, K. Saitoh, D. Mcclane,T. Hawkins, P. Foy, G.C. Gu, and L. Dong, "Mode Area Scaling with All-solid Photonic Bandgap Fibers,", Optics Express 20, 26363-26372 (2012).

[52] G. Gu, F. Kong, T.W. Hawkins, J. Parsons, M. Jones, C. Dunn, M.T. Kalichevsky-Dong, K. Saitoh, and L. Dong, "Ytterbium-doped large-mode-area all-solid photonic bandgap fiber lasers," Optics Express 22, 13962-13968(2014).